25th ABCM International Congress of Mechanical Engineering
October 20-25, 2019, Uberlândia, MG, Brazil

COB-2019-0908
LOCALIZATION OF ANISOTROPIC BEARINGS THROUGH THE MODIFICATION OF THE SHAPE AND DIRECTIVITY INDEX (*SDI*)

Lucas Rangel de Oliveira
Gilberto Pechoto de Melo
Department of Mechanical Engineering. São Paulo State University "Júlio de Mesquita Filho", Ilha Solteira, 15385000, Brazil.
lucas.r.oliveira@unesp.br
gilberto.pechoto@unesp.br

Abstract. *This work presents the design of an index that assists in locating anisotropic bearings in rotating shafts through the Shape and Directivity Index (SDI) information. The equation of motion of the rotor uses complex notation in order to separate the contributions of the forward and backward whirl modes. By manipulating SDI in the HSV color model, a metric scale, visualized on a color map, is developed to locate the anisotropy caused by anisotropic bearings. Good results demonstrate the efficiency and robustness of the new index for several rotor operation conditions. This damage metric contributes to anisotropy localization methods in rotating systems.*

Keywords: *rotordynamics, shape and directivity index, complex modal analysis, backward and forward whirl*

1. INTRODUCTION

Depending on the system conditions, the unbalance force can excite a rotor with anisotropic bearings in forward, backward or mixed precession modes (Dias Jr et al., 2004; Kessler and Kim, 2002; Lang et al., 2015). In this context, the rotordynamics analysis using complex notation has proved to be a powerful tool. This methodology helps to understand the precession modes and makes it possible to separate the forward and backward precession components.

Han and Lee (1999) introduced the *SDI* to quantitatively describe the orbit shape and the direction of the precession at a position of the rotor. *SDI* signal defines the direction of the precession while the absolute value defines the orbit shape. Dias Jr and Allemang (2001) introduced *SDI* Plot, a simple and efficient tool that clearly shows the direction (forward or backward) and shape (circular, elliptic or rectilinear) of any rotor position at any speed of rotation through a map of colors.

Subsequently, Dias Jr et al. (2004) proved, numerically and experimentally, the occurrence of mixed operational modes, which means that the rotor can be precessed forward over one part of the shaft and reverse precession over another part in the same time. A color map, called *SDI* Plot, was introduced and presented as a tool in viewing the directivity and shape of any rotor node at any rotational speed. However, these works that show the *SDI* Plot do not present the computational tool or the code used for its construction (Dias Jr and Allemang, 2001; Dias Jr et al., 2004).

This paper presents a mathematical formulation that makes it possible to construct a color map similar to the presented in the literature. In addition, a standard behavior is observed in the *SDI* values that allows the development of a metric index to support in locating the anisotropy caused by the bearings.

2. MATHEMATICAL SYSTEM MODELING

The system consists of a flexible shaft, two disks, supported by three bearings and excited by an unbalance mass positioned on the disk 1, Fig. 1(a). The Finite Element Method is used in the formulation of the equations of motion. The shaft is divided into N (N = 16) nodes with four degrees of freedom at each node, Fig. 1(b). The parameters are described at Tab. 1.

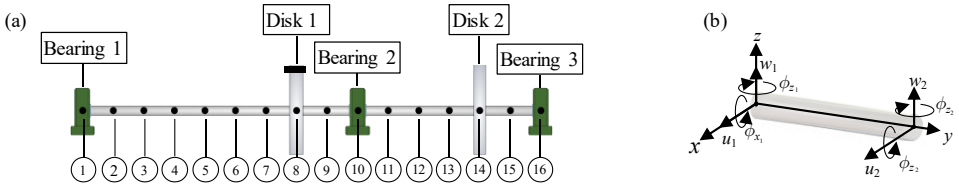

Figure 1. (a) Structure model discretized by finite elements. (b) Model of the finite element of the shaft.

Table 1. Physical parameters of the cracked rotor.

Parameters	Values	Parameters	Values
Length of the shaft	0.75 m	Disk thickness	0.02 m
Radius of the shaft	0.005 m	Young's modulus	$2.1\ 10^{11}$ N m^{-2}
Outer diameter of the disks	0.20 m	Poisson ratio	0.3
Inner diameter of the disks	0.010 m	Unbalance	10^{-07} kg.m

The assembly of the overall matrix ensures that each row and column of the element matrix (mass, stiffness, and damping) is identified by the corresponding degree of freedom and placed in their appropriate positions. After this procedure, the equation of motion is written according to Lalanne and Ferraris (1998) by

$$\boldsymbol{M}\,\ddot{\vec{q}}(t)+\left(\boldsymbol{D}+\Omega\boldsymbol{G}\right)\dot{\vec{q}}(t)+\boldsymbol{K}\,\vec{q}(t)=\vec{f}(t) \tag{1}$$

where $\vec{q}\in\mathbb{R}^{4n}$ is the nodal displacement vector, $\vec{q}_i=\left\{x_i\ z_i\ \phi_i^x\ \phi_i^z\right\}^T$ is the vector that includes the translational and rotational displacement for the node $i=1,2,\ldots,n$, n is the number of nodes, $\vec{f}\in\mathbb{R}^m$ is the excitation vector (which considers the unbalance force and the gravitational force), $\boldsymbol{M},\boldsymbol{D},\boldsymbol{G}$ and $\boldsymbol{K}\in\mathbb{R}^{4n\times 4n}$ are the global matrices of mass, damping, gyroscopic and stiffness, m is the number of inputs and Ω is the angular speed.

The transformation of the real-to-complex response vector is given by (Dias Jr et al., 2004; Han and Lee, 1999)

$$\begin{Bmatrix}\vec{p}(t)\\ \vec{p}^{\,*}(t)\end{Bmatrix}=\boldsymbol{T}^{-1}\vec{q}(t) \tag{2}$$

where each term is given by

$$\begin{Bmatrix}\vec{p}(t)\\ \vec{p}^{\,*}(t)\end{Bmatrix}=\begin{Bmatrix}\vec{p}^{\,l}(t)\\ \vec{p}^{\,\phi}(t)\\ \vec{p}^{\,l*}(t)\\ \vec{p}^{\,\phi*}(t)\end{Bmatrix}=\begin{Bmatrix}z_i(t)+jx_i(t)\\ \phi_i^x(t)+j\phi_i^z(t)\\ z_i(t)-jx_i(t)\\ \phi_i^x(t)-j\phi_i^z(t)\end{Bmatrix};\quad \vec{q}(t)=\begin{Bmatrix}x(t)\\ z(t)\\ \phi^x(t)\\ \phi^z(t)\end{Bmatrix};\quad \boldsymbol{T}^{-1}=\begin{bmatrix}j & 1 & 0 & 0\\ 0 & 0 & 1 & j\\ -j & 1 & 0 & 0\\ 0 & 0 & 1 & -j\end{bmatrix};\quad \boldsymbol{T}=\frac{1}{2}\begin{bmatrix}-j & 0 & j & 0\\ 1 & 0 & 1 & 0\\ 0 & 1 & 0 & 1\\ 0 & -j & 0 & j\end{bmatrix}$$

where j $\left(j=\sqrt{-1}\right)$ is the complex variable, x_i and z_i are the translational displacements and ϕ_i^x and ϕ_i^z are the angular displacements around the directions x (horizontal) and z (vertical) of each node.

The motion equation in complex coordinates is given compactly by:

$$\boldsymbol{M}_a\begin{Bmatrix}\ddot{\vec{p}}(t)\\ \ddot{\vec{p}}^{\,*}(t)\end{Bmatrix}+\boldsymbol{D}_a\begin{Bmatrix}\dot{\vec{p}}(t)\\ \dot{\vec{p}}^{\,*}(t)\end{Bmatrix}+\boldsymbol{K}_a(t)\begin{Bmatrix}\vec{p}(t)\\ \ddot{\vec{p}}^{\,*}(t)\end{Bmatrix}=\begin{Bmatrix}\vec{g}(t)\\ \vec{g}^{\,*}(t)\end{Bmatrix} \tag{3}$$

where $\boldsymbol{M}_a=\boldsymbol{T}^{-1}\boldsymbol{M}\boldsymbol{T}$, $\boldsymbol{K}_a=\boldsymbol{T}^{-1}\boldsymbol{K}\boldsymbol{T}$ and $\boldsymbol{D}_a=\boldsymbol{T}^{-1}\boldsymbol{D}\boldsymbol{T}$ are the matrices of Eq. (1) using the complex notation.

Considering a rotor with anisotropic characteristics operating in constant rotation and steady-state conditions, the displacement, $\vec{p}(t)$, and the external force, $\vec{g}(t)$, in complex notation can be decomposed in its forward components, $\vec{P}_f$ and $\vec{G}_f$, and backward components, $\vec{P}_b$ and $\vec{G}_b$, as follows (Dias Jr et al., 2004; Han and Lee, 1999)

$$\vec{p}(t)=\vec{P}_f e^{j\Omega t}+\vec{P}_b e^{-j\Omega t} \tag{4}$$

$$\vec{g}(t)=\vec{G}_f e^{j\Omega t}+\vec{G}_b e^{-j\Omega t} \tag{5}$$

Substituting Eqs. (4)-(5) and their respective complex quantities into Eq. (3), it is possible to separate the matrices of the system, the response vectors and the excitation vectors by

$$\left(-\Omega^2\boldsymbol{M}_a+j\Omega\boldsymbol{D}_a+\boldsymbol{K}_a\right)\begin{Bmatrix}\vec{P}_f\\ \vec{P}_b^{\,*}\end{Bmatrix}=\begin{Bmatrix}\vec{G}_f\\ \vec{G}_b^{\,*}\end{Bmatrix} \tag{6}$$

3. MATHEMATICAL FORMULATION FOR *SDI PLOT*

The forward $\left(\vec{P}_f\right)$ and backward $\left(\vec{P}_b\right)$ components can be assembled in a parameter, Shape and Directivity Index (*SDI*), defined by Han and Lee (1999) by

$$-1 \le SDI = \frac{|P_f| - |P_b|}{|P_f| + |P_b|} \le 1 \tag{7}$$

The *SDI* applied in the study of anisotropic bearings defines the motion characteristics of the node. The signal defines the direction of motion and the absolute value defines the shape of the orbit, summarized in Tab. 2.

Table 2. Relationship between *SDI* values and shaft motion.

Parameter *SDI*	Direction of motion	Shape of the orbit
$SDI = 1$	Forward	Circular
$1 > SDI > 0$	Forward	Elliptical
$SDI = 0$	Forward	Rectilinear
$0 > SDI > -1$	Backward	Elliptical
$SDI = -1$	Backward	Circular

SDI values can be more easily viewed through a color map, called *SDI* Plot. However, the works that show the use of this tool do not present information for its development. This paper proposes a mathematical formulation to develop the color map, like that shown in Dias Jr et al. (2004). As the color map shown in this paper differs in some color of the hue (for example, the presence of magenta and cyan) from the map presented by Dias Jr et al. (2004), the authors maintained the same name but written differently, such as SDI_{Plot}.

In this work, the construction of the SDI_{Plot} color map is done by manipulating the values of the *SDI* vector in the HSV color system. The HSV model is composed of hue, saturation and value components. The hue represents the pure color with maximum saturation and luminosity. This parameter allows to express all existing colors, starting in red, through orange, yellow, green, blue, purple, magenta, and back to red. These colors are quantified at an angular value between 0 and 360 degrees, or between 0 and 1, as shown in Fig. 2(a) and Table 3 (Buss, 2003). The saturation indicates the higher or lower intensity of the tonality. The less saturated, the smoother, grayer the image appears. The more saturated, the more "alive", Fig. 2(b). The value represents the amount of light that affects the color. The lighter or darker color indicates the amount of light it contains, Fig. 2(c) (Buss, 2003).

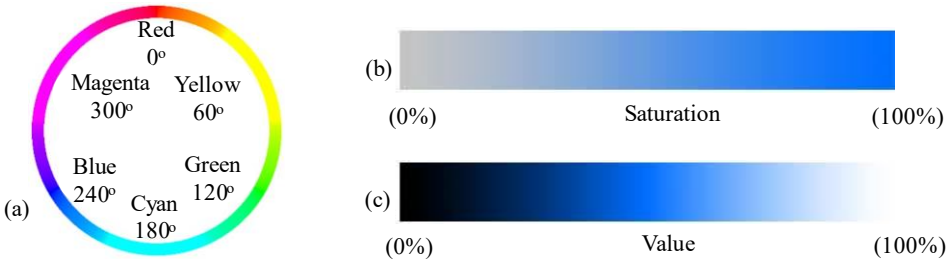

Figure 2. (a) Color gradient in the HSV model. (b) Saturation and (c) Scale of value for the blue color.

Table 3. Relation of the pure colors (hue) in the HSV model and its angular and scalar values.

Pure color	Red	Yellow	Green	Cyan	Blue	Magenta	Red
Angle (0º-360º)	0	60	120	180	240	300	360
HSV (0-1)	0	60/360	120/360	180/360	240/360	300/360	1

Keeping saturation and value at 100%, the color map is obtained from the following equation

$$\begin{aligned} SDI_{Plot} &= \left\{(1 - SDI)\left[\left(HSV_{\min^+}\right) - \left(HSV_{\max^+}\right)\right]\right\} + HSV_{\max^+}, \quad \text{for } SDI > 0 \\ SDI_{Plot} &= \left\{(1 - |SDI|)\left[\left(HSV_{\min^-}\right) - \left(HSV_{\max^+}\right)\right]\right\} + HSV_{\max^-}, \quad \text{for } SDI < 0 \end{aligned} \tag{8}$$

where $SDI_{Plot} \in \mathbb{R}^{n\times\beta}$ are the values of the *SDI* parameter in the HSV color model, β is the size of the frequency vector, HSV_{max^+} and HSV_{min^+} represent the value for the maximum and minimum absolute value of the *SDI* for the interval $0 < SDI \leq 1$, and HSV_{max^-} and HSV_{min^-} for the interval $-1 \leq SDI < 0$.

For the isotropic system, there is no backward component in the response, shown in the directional unbalance response, Fig. 3(a). Thus, the SDI_{Plot} have an exclusively green color, Fig. 3(b). Figures 3-4 (c) shows the color scale that correlates with the anisotropy values SDI shown in Table 2.

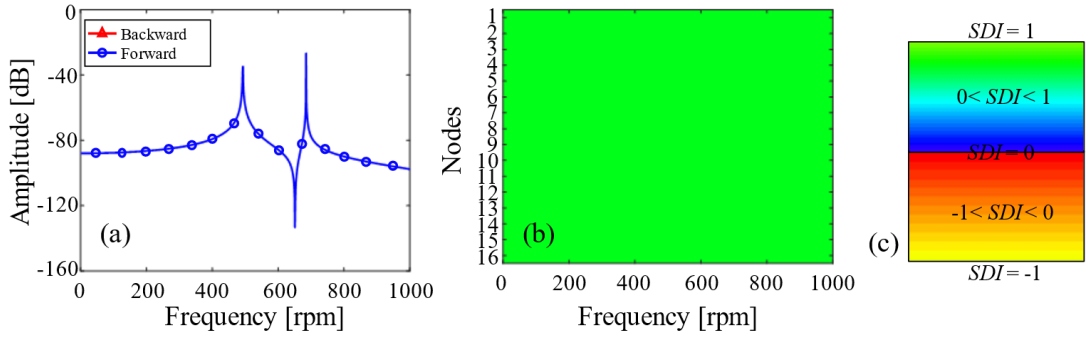

Figure 3. (a) Directional Unbalance Response for the isotropic system. (b) SDI_{Plot} for the isotropic system. Color scale of the SDI_{Plot}.

However, if there is anisotropy in the bearings – in this case the horizontal stiffness has been decreased from 20 kN / m to 16 kN / m – there is the appearance of the backward component, Fig. 4(a), indicated by the change on the color map, Fug. 4(b).

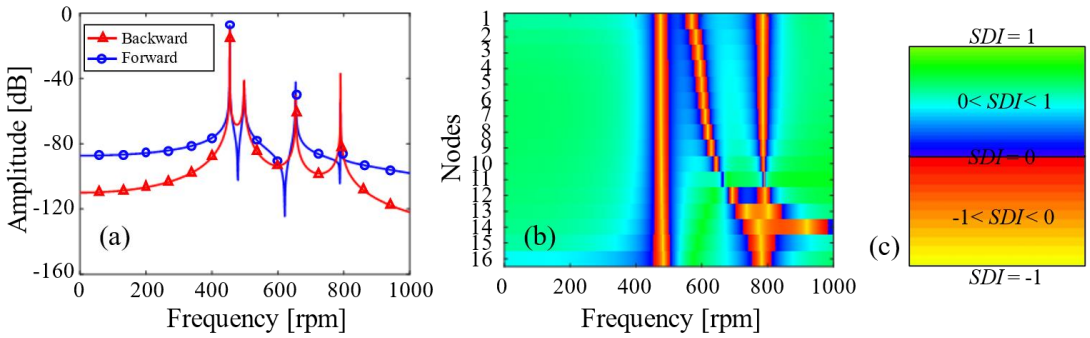

Figure 4. (a) Directional Unbalance Response for the anisotropic system. (b) SDI_{Plot} for the anisotropic system. Color scale of the SDI_{Plot}.

The backward component can be catastrophic for the rotor. In this case, the damping in the bearings can decrease (even eliminate) regions of backward precession. Figure 5 illustrates the same case as Fig. 4, where Fig 5 (a) does not consider bearing damping and Fig. 5 (b) considers 100 Ns / m damping in bearings.

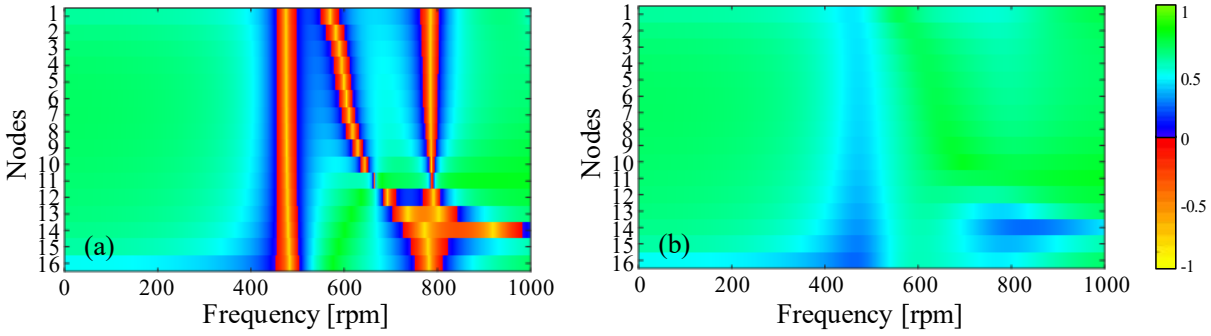

Figure 5. SDI_{Plot} for the anisotropic rotor (a) not considering damping (b) considering damping.

Figure 6 shows the orbits of nodes 1, 11, and 16 for the four speeds, covering regions of forward and backward precession: 100, 497, 592, and 808 rpm. The marker (blue circle) inserted in the orbit delimits the end of the signal to make it easier to see the direction of rotation.

During rotation of 100 rpm (green color in SDI_{Plot}) orbits have circular shape and forward precession mode, while during rotation of 497 rpm (yellow color in SDI_{Plot}) orbits have circular shape and backward precession mode. However, the speeds of 592 and 808 rpm show variations in orbit shape (circular and ellipsoidal) as well as changes in mode directionality, confirming the occurrence of mixed modes.

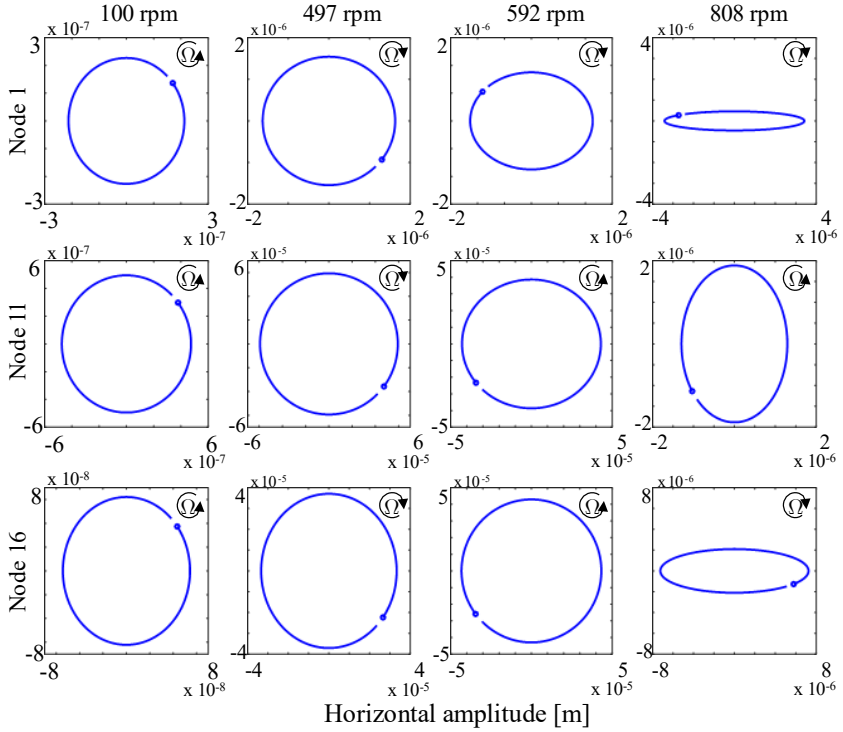

Figure 6. Rotor orbits for forward, backward and mixed precession regions.

4. A NEW INDEX TO LOCATE ANISOTROPY

By analyzing the SDI_{Plot} vector, it was noted that the largest value lies in the positions of the anisotropic bearings. However, depending on the system, anisotropy may vary little in absolute values, but relative values may be considerable. Therefore, it is proposed to design an index, called *AII* (Anisotropy Identification Index), to locate the nodes with the greatest anisotropy. The mathematical formulation is given by

$$AII = \left\{ \left| \frac{\min\left(SDI_{Plot}\right) - SDI_{Plot}}{\min\left(SDI_{Plot}\right) - \max\left(SDI_{Plot}\right)} \right| \left[\left(HSV_{\max}\right) - \left(HSV_{\min}\right) \right] \right\} + HSV_{\min} \tag{9}$$

For the system analyzed in chapter 5, Fig. 7 illustrates the difference between *SDI* values and *AII* values.

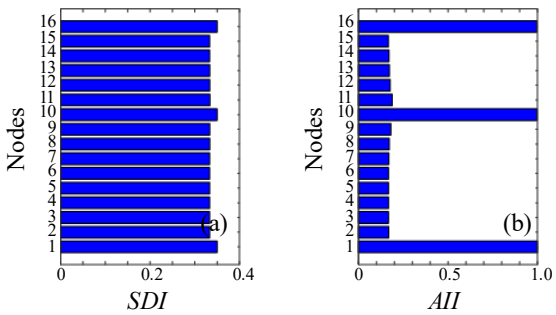

Figure 7. Anisotropy of the nodes by (a) *SDI* values and (b) *AII* values.

In order to simply identify nodes with the highest and lowest anisotropy, this index is shown by a color map, called AII_{Plot}. *AII* values are considered in the HSV color system and the meaning of the colors is shown on a scale by Fig. 8.

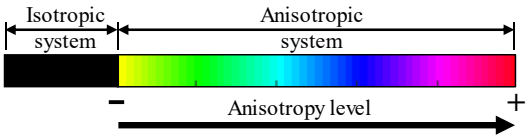

Figure 8. Representation of the AII_{Plot} color range.

This color map is only qualitative, ranging from a minimum level of anisotropy (zero value) to a maximum level of anisotropy (unit value). For an isotropic system, the generated is black, to avoid mistakes with shades of yellow.

The representation of the *SDI* values directly in the HSV color model is not effective because: (1) by the small difference between the absolute maximum and minimum values, sometimes in the third decimal place, the color difference would be given by shades very close to the same color and (2) the value zero and one represent the same color, red, making it difficult to distinguish colors in the HSV model.

5. RESULTS AND CONCLUSION

In order to analyze the efficiency and robustness of the index, two situations are evaluated: (1) varying the position of the bearings and (2) varying the values of the coefficients of the bearings. For the first situation, the bearing stiffness in horizontal direction is decreased from 20 to 16 MN/m – the change in order of the coefficients is explained in Fig. 11.

Four situations are considered in this first analysis. The bearing positions on the shaft are described in Tab. 4.

Table 4. Positioning of the bearings evaluated in Fig. 9.

	Bearing 1	Bearing 2	Bearing 3
Case (a)	1	10	16
Case (b)	4	12	15
Case (c)	6	10	12
Case (d)	10	12	16

The *AII* values for each node are represented in a bar graph, Fig. 9. This shows that the highest index values are in the bearing nodes, identifying the most anisotropic positions.

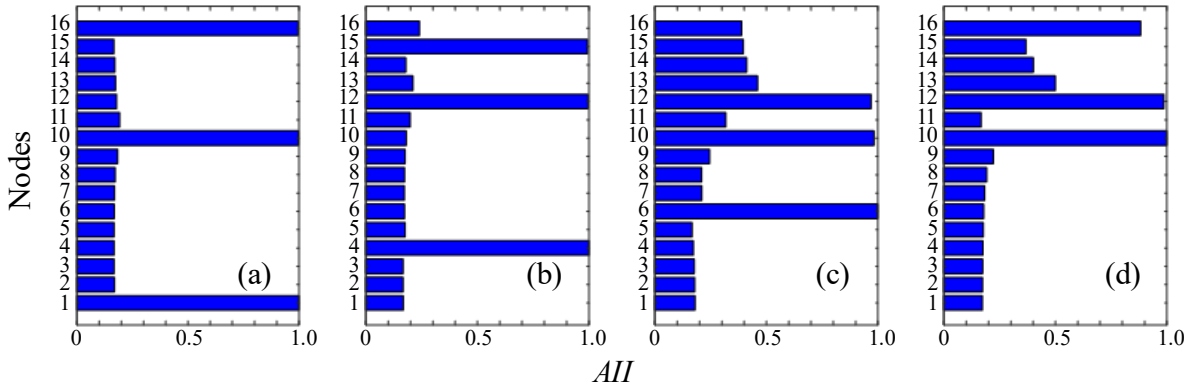

Figure 9. *AII* performance for different bearing positions.

In addition, the node anisotropy difference can be visualized by the color map mentioned above, Fig. 10. Note that, even in case (d) the rotor is in balance, considerably changing the system configuration. The success to locate anisotropic bearings is observed, where the red color indicates the highest degree of anisotropy in the positions of the bearings.

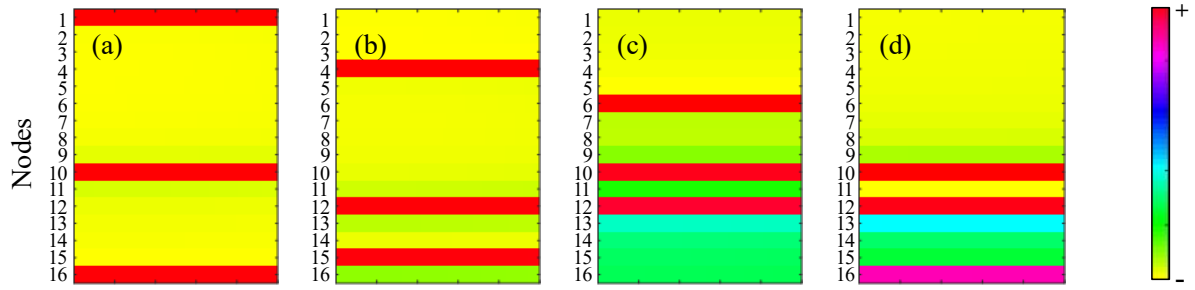

Figure 10. AII_{Plot} performance for different bearing positions.

For the second analysis the bearings are fixed at the positions described for case (a) of Tab. 4. The values of the bearing coefficients are described in Table 5.

Table 5. Bearing coefficients evaluated in Fig. 11.

	Bearing 1		Bearing 2		Bearing 3	
	Stiffness	Damping	Stiffness	Damping	Stiffness	Damping
Case (a)	k_{xx} = 20 MN/m k_{zz} = 20 MN/m		k_{xx} = 20 MN/m k_{zz} = 20 MN/m		k_{xx} = 20 MN/m k_{zz} = 20 MN/m	
Case (b)	k_{xx} = 16 MN/m k_{zz} = 20 MN/m	c_{xx} = 100 Ns/m c_{zz} = 100 Ns/m	k_{xx} = 16 MN/m k_{zz} = 20 MN/m	c_{xx} = 100 Ns/m c_{zz} = 100 Ns/m	k_{xx} = 16 MN/m k_{zz} = 20 MN/m	c_{xx} = 100 Ns/m c_{zz} = 100 Ns/m
Case (c)	k_{xx} = 15 MN/m k_{zz} = 20 MN/m		k_{xx} = 17 MN/m k_{zz} = 20 MN/m		k_{xx} = 18 MN/m k_{zz} = 20 MN/m	
Case (d)	k_{xx} = 16 kN/m k_{zz} = 20 kN/m		k_{xx} = 16 kN/m k_{zz} = 20 kN/m		k_{xx} = 16 kN/m k_{zz} = 20 kN/m	

For the second analysis the bearings are fixed at the positions described for case (a) of Table 4. The values of the bearing coefficients are described in Table 5. For the isotropic system, Eq. (9) becomes undefined, with no values for *AII*, illustrated in Fig 11(a).

Case (b) is similar to case (a) of Fig. 9, but considering bearing damping. Note that it does not influence the location. Case (c) considers for each bearing a different anisotropy. Note that the *AII* values vary according to the intensity of anisotropy.

Case (d) is the same system presented in chapter 3. An improvement in this index is that: for soft bearing systems – when bearing stiffness is low relative to shaft stiffness – the *AII* performance is low. For this reason, for case (d), the index did not locate the anisotropic bearings. However, it provides good results for stiff bearing systems – when the bearings are much stiffer than the shaft.

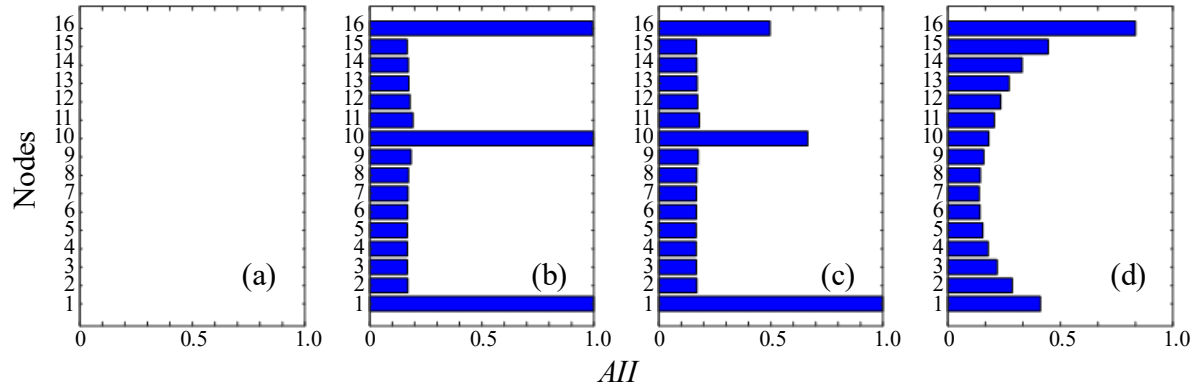

Figure 11. *AII* performance for different anisotropy values.

The same notes can be seen in Fig. 12 through the color map. As for the case (a) the system is isotropic, all nodes are black. In case (c), where there are different anisotropies, the colors vary according to the intensity of anisotropy.

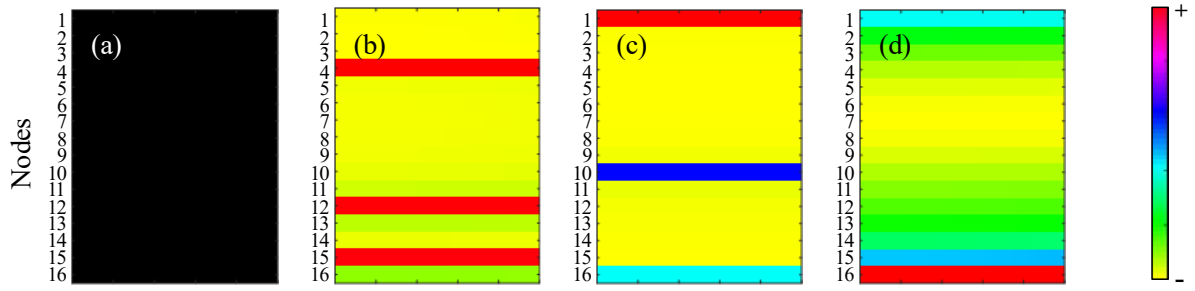

Figure 12. AII_{Plot} performance for different anisotropy values.

As a first contribution, this paper presents a mathematical formulation for the elaboration of the *SDI* Plot color map. In addition, based on the *SDI* modification, an index for anisotropy localization is presented and good results under different operating conditions are noted.

6. ACKNOWLEDGMENTS

This study was financed in part by the CAPES - Finance Code 001.

7. REFERENCES

Buss, S.R., 2003. 3-D Computer Graphics: A Mathematical Introduction with OpenGL. Cambridge University Press, San Diego.

Dias Jr, M., Allemang, R.J., 2001. “Some Insights into the Simultaneous Forward and Backward Whirling of Rotors”. *In Proceedings of the XIX IMAC - Internationa Modal Analysis Conference*, San Antonio, United State.

Dias Jr, M., Idehara, S.J., Mesquita, A.L.A, and Miranda, U.A., 2004. “On the Simultaneous Forward and Backward Whirling in Flexible Rotors: Numerical Analysis and Experimental Verification.” *Australian Journal of Mechanical Engineering*, Vol. 1, No. 2, pp. 113–22.

Han, Y.S., and Lee, C.H., 1999. “Directional Wigner Distribution for Order Analysis in Rotating/Reciprocating Machines.” *Mechanical Systems and Signal Processing*, Vol. 13, No. 5, pp. 723–737.

Kessler, C., Kim, J., 2002. “Vibration analysis of rotors utilizing implicit directional information of complex variable descriptions”. *Journal of Vibration and Acoustics*, Vol. 124, No. 10, pp. 340-349.

Lalanne, M., and Ferraris, G., 1998. *Rotordynamics Prediction in Engineering*. John Wiley & Sons Ltd, Chichester, 2nd edition.

Lang, G., Liao, Y., Liu, Q., Lin, J., 2015. “Study on the precession orbit shape analysis-based linear fault qualitative identification method for rotating machinery”. *Journal of Sound and Vibration*, Vol. 335, pp. 321–337

Lee, C.W., 1991. “A Complex Modal Testing Theory for Rotating Machinery.” *Mechanical Systems and Signal Processing*, Vol 5, No. 2, pp. 119–37.

8. RESPONSIBILITY NOTICE

The authors are the only responsible for the printed material included in this paper.